

This document is the unedited author's version of a Submitted Work that was subsequently accepted for publication in ACS Applied materials and interfaces, copyright © American Chemical Society after peer review. To access the final edited and published work, see <https://pubs.acs.org/doi/10.1021/acsami.3c17625>.

A Gas-Steam Route to Mesoporous Open Metal-Organic Framework Cages Enhancing Flame Retardancy and Smoke Suppression of Polyurea

Kunpeng Song^a, Xue Bi^a, Chuang Yu^a, Ye-Tang Pan^{a*}, Henri Vahabi^b, Vera Realinho^c, Jiyu He^{a*}, Rongjie Yang^a

^aNational Engineering Research Center of Flame Retardant Materials, School of Materials Science & Engineering, Beijing Institute of Technology, Beijing 100081, PR China

^bUniversité de Lorraine, CentraleSupélec, LMOPS, F-57000 Metz, France

^cPoly2 Group, Department of Materials Science and Engineering, School of Industrial, Aerospace and Audiovisual Engineering of Terrassa, Universitat Politècnica de Catalunya (UPC BarcelonaTech), C/ de Colom, 11, 08222 Terrassa, Spain

*Corresponding authors: Ye-Tang Pan; Jiyu He.

E-mail address: pyt@bit.edu.cn; hejiyu@bit.edu.cn

Abstract:

Up to now, metal-organic frameworks (MOFs) with open nanostructures have shown outstanding capabilities in trapping smoke particles compared to original MOFs. However, only a few MOF-based strategies have been reported to synthesize hierarchical porous cages thus far, which are mainly restricted to environmentally unfriendly wet-chemistry liquid methods. Herein, as a proof-of-concept, a gas-

steamed metal–organic–framework approach was designed to fabricate a series of cheese-like open cages with hierarchical porosity. Briefly, zeolitic imidazolate framework-67 (ZIF-67) was employed as the precursor and phytic acid as the etching agent. Abandoning the conventional wet chemical method, the coordination bond of ZIF-67 was cleaved by acidic steam, forming an open framework with high specific surface area and hierarchical porous structure. The universality of this method was also confirmed by the selection of different etchants. Impressively, they also show outstanding fume-toxic adsorption capability and labyrinth effects based on abundant and complex porous channels. At only 5 wt% loading, $\text{Co}_3\text{O}_4@open\ ZIF-67\ cage-2$ ($\text{Co}_3\text{O}_4@OZC-2$) imparted polyurea (PUA) composites with 21.2% limiting oxygen index, and the peak of heat release rate, total heat release and total smoke production were reduced by around 37.5%, 25.5% and 40.4%, respectively, compared to neat PUA. This work will shed light on the advanced structural design of polymer composites with high fire safety, especially smoke suppression performance, so as to obtain more feasible applications.

Keywords: metal-organic framework, mesoporous cages, smoke suppression, polyurea, fire safety

1. Introduction

Polyurea (PUA) is a polymer elastomer generated by the reaction of an isocyanate component and an amino compound component. Polyurea elastomers have excellent corrosion resistance, mechanical properties and wear resistance, and are widely utilized in marine anticorrosion, building waterproofing and equipment protection.¹⁻³ However, as with other polymeric materials, the poor fire retardancy of PUA poses a potential smoke hazard especially in high temperature environments.⁴⁻⁶ Adding flame retardants (FRs) to the polymer matrix is one of the most effective strategies for improving the fire safety of

composites.⁷⁻⁹ Heat and smoke toxicity released from the polymer decomposition are considered to be the primary factors contributing to fire hazards.^{10, 11} Numerous FRs have been designed and function well in fire safety especially for the suppression of combustion heat.¹² However, there are few reports of FRs designed for smoke suppression characteristics.¹³⁻¹⁵ Therefore, more attention should be devoted to the design of functional FRs with both flame retardant and smoke suppression properties.

Emerging as a class of promising porous crystalline coordination compounds, metal–organic frameworks (MOFs) have flourished as attractive precursors/templates for the fabrication of various functional materials, and are broadly employed in catalysis, photovoltaics, energy storage, and others.¹⁶⁻¹⁸ Besides, MOFs with the favorable thermal stability and catalytic activity are considered as an ideal FRs and have great potential in improving the flame retardancy and smoke suppression of polymers.¹⁹ Specifically, as a novel porous material, the large pore volume and specific surface area of MOFs exhibit superior adsorption properties, which can capture smoke and toxic gases released during the composite combustion. In addition, MOFs with abundant transition metal sites can provide a large number of active catalytic centers, so as to play a better catalytic charring effect. As a catalyst in the CO-catalytic oxidation reaction, transition metals can reduce the release of CO and promote the production of CO₂.²⁰

Considering that smoke release is primarily caused by incomplete combustion of cracked volatiles during polymer burnout, and smoke particles too large in size to be efficiently captured by microporous MOFs.²¹ So far, the synthesis of MOFs with hierarchical porous and open nanostructures is considered as an effective approach to solve the above problem, which improves the capture capacity of MOFs for different sizes of smoke particles as well as toxic gases.²² Yuan et al.²³ prepared a hydrophobic MOF-based flame retardant (S-Fe-MOF) inspired by the particular surface structure of lotus leaves. Specifically,

ammonia aqueous solution was used as the etchant to realize the pore expansion of the iron-metal organic framework (Fe-MOF) for the adsorption and loading of triethyl phosphate and polydimethylsiloxane. Compared with the pristine Fe-MOF, the water contact angle of S-Fe-MOF increased from 31.9° to 122.0°, exhibiting remarkable hydrophobicity. And S-Fe-MOF significantly enhanced the flame retardancy and thermal stability of polystyrene composites at 3 wt% loading, with a 46.0% and 12.3% reduction in peak of heat release rate (pHRR) and total heat release (THR), respectively. Unfortunately, the pore architecture of remaining Fe-MOF and the fume-toxic release behavior of the composite were not studied in detail. Zhao et al.²⁴ also employed a similar method to prepare macroporous MIL-53(Fe) metal-organic frameworks (pore size between 20 and 200 nm) for adsorbing triethyl phosphate. The pHRR, THR, and peak carbon dioxide production rate (PCOPR) of polystyrene composites mixed with 3 wt% flame retardant filler decreased by 24.7%, 12.7%, and 40.7% respectively, and the smoke density ranking decreased by 26.1%, compared with pure polystyrene. However, this work does not clearly explain the influence of flame retardants with macroporous structure on smoke and toxic substances, but only intends to achieve the loading of small molecule flame retardants through larger pore diameters. Recently, Dai et al.²⁵ reported a hierarchical porous organophosphorus modified hollow bimetallic organic frameworks (W-Zr-MOF-DOPO) employing zirconium-based MOFs (Zr-MOF-NH₂) as a template and sodium tungstate as an etchant. The transition metals and hierarchical pores of the as-prepared FRs can effectively facilitate the catalytic charring and adsorption of pyrolytic volatiles. In addition, P element also plays a flame retardant role in condensed phase and gas phase. Thus, only 3 wt% addition of W-Zr-MOF-DOPO can impart the epoxy composite 32.2% limiting oxygen index (LOI) and pass the UL-94 V-0 rating. In particular, the total smoke production (TSP) and pHRR of the epoxy

composites were significantly reduced by 36.1% and 57.8%, respectively, compared to the pure epoxy. However, they encountered intractable obstacles, such as the complex process, tightly controlled reaction conditions, and poor universality.

In particular, specific nanostructured MOFs are often difficult to tune in terms of size and shape due to their excellent physical and chemical stability.²⁶ So far, only a few MOFs-based strategies have been reported for the preparation of pre-defined MOFs structures, from which they are mainly confined to wet-chemical liquid methods.²⁷ This class of traditional syntheses is performed in liquid phase with environmentally unfriendly organic solvents, and the created cage structures are usually an enclosed-wall structures, which are not conducive to mass transfer and adsorption properties.²⁸ Based on the breakthrough of the concept of traditional wet synthesis, it is urgent to explore new synthesis methods for constructing hierarchical porous open skeleton for practical application.

Herein, inspired by steaming Chinese bun process, we have developed a convenient gas-steamed metal-organic framework (GSM) approach to fabricate cheese-like cages with open-wall and hierarchical porosity. Within a confined space of phosphoric acid (H_3PO_4) vapor formed by the decomposition of phytic acid ($\text{C}_6\text{H}_{18}\text{O}_{24}\text{P}_6$), large controlled defects tend to occur on the ZIF-67 crystals, leading to the generation of open cages. Meaningfully, based on this synthetic strategy, similar structures can also be acquired by replacing different etchants (e.g., low-boiling acids or bases and compounds that decompose to release low-boiling acids or bases). This hierarchical porous architecture can create large specific surface area and pore channels for enhancing smoke capture, which is also validated by targeted performance evaluation. To our knowledge, the study of hierarchical porous MOFs cages based on different pore diameter distributions with polymeric materials for enhancing their fire safety has not been

reported before. As expected, open ZIFs cages all showed high specific surface area (more than 1000 m²/g) and favorable thermal stability. Impressively, both microporous and mesopore-dominated hierarchical structures have superior flame retardant and smoke trapping capabilities, especially Co₃O₄@OZC-2. And the pHRR, THR and TSP of as-prepared PUA composites were reduced by 37.5%, 25.5%, and 40.4%, respectively, compared to the pure PUA. More importantly, this open cage fabrication strategy to improve smoke suppression performance by regulating adsorption capability and catalytic activity is also suitable for other functional materials. In this work, this systematic work suggests more astute approaches for the design of MOF-derived open cage with hierarchical pores with high efficacy in the polymeric materials to mitigate the fire hazards, especially smoke toxic hazards.

2. Experimental section

2.1 Materials

Cobaltous nitrate hexahydrate (Co(NO₃)₂·6H₂O, 98.0%) and 2-methylimidazole (2-MeIM, 99.0%) were acquired from Tianjin Kemiou Chemical Reagent Co., Ltd. Polyurea component A and component B were supplied by Chengdu Shangtai Technology Co., Ltd, and their molecular structural formulas are shown in **Figure S1**. Deionized water and absolute methanol (AR) were purchased from the Meryer (Shanghai) Chemical Technology Co., Ltd. Urea (99.0%) and ammonia solution (AR) were acquired from the Beijing Chemical Plant. Phytic acid (PA, 70.0% (w/w) in H₂O), phosphoric acid (AR), and glacial acetic acid (≥99.8%) were all provided by Shanghai Aladdin Biochemical Technology Co., Ltd.

2.2 Preparation of Co₃O₄@open ZIF-67 cages (Co₃O₄@OZCs)

The preparation process of sample is schematically illustrated in **Scheme 1a**. First, ZIF-67 crystals

were synthesized under ambient conditions with reference to the typical method previously and employed as precursors for the fabrication of $\text{Co}_3\text{O}_4@\text{OZCs}$ materials.²⁹ The as-prepared ZIF-67 crystals (0.10 g) were dispersed evenly in absolute methanol (20 mL) with the assistance of ultrasound (200 W, 40 KHz) for 30 min. It was then uniformly coated on the inner walls of 50 mL isotope vials and dried at 120 °C for 12 h. Subsequently, the ZIF-67 coated isotope vial was placed in a Teflon reactor containing PA solution (50.0% (w/w) in H_2O) and reacted at 130 °C for a specific time (2 h, 4 h, 6 h, and 12 h) (**Figure S2**). Finally, the products on the inner wall of the isotope vial were collected and centrifuged with absolute methanol, and then transferred to a blast oven for drying at 80 °C for 12 h. The corresponding samples were designated as $\text{Co}_3\text{O}_4@\text{open ZIF-67 cages-x}$ ($\text{Co}_3\text{O}_4@\text{OZC-x}$, $x = 2, 4, \text{ and } 6$, and x is defined as the number of hours of reaction time) and nano- Co_3O_4 (12 h after etching), respectively.

2.3 Preparation of $\text{Co}_3\text{O}_4@\text{open ZIF-67 cages}$ with phosphoric acid as etchant ($\text{Co}_3\text{O}_4@\text{OZC-H}_3\text{PO}_4$)

Details of this section are in Supplementary Material.

2.4 Preparation of $\text{Co}_3\text{O}_4@\text{open ZIF-67 cages}$ with acetic acid as etchant ($\text{Co}_3\text{O}_4@\text{OZC-CH}_3\text{COOH}$)

Details of this section are in Supplementary Material.

2.5 Preparation of $\text{Co}_3\text{O}_4@\text{open ZIF-67 cages}$ with ammonia solution as etchant ($\text{Co}_3\text{O}_4@\text{OZC-NH}_3 \cdot x\text{H}_2\text{O}$)

Details of this section are in Supplementary Material.

2.6 Preparation of $\text{Co}_3\text{O}_4@\text{open ZIF-67 cages}$ with urea as etchant ($\text{Co}_3\text{O}_4@\text{OZC-(NH}_2)_2\text{CO}$)

Details of this section are in Supplementary Material.

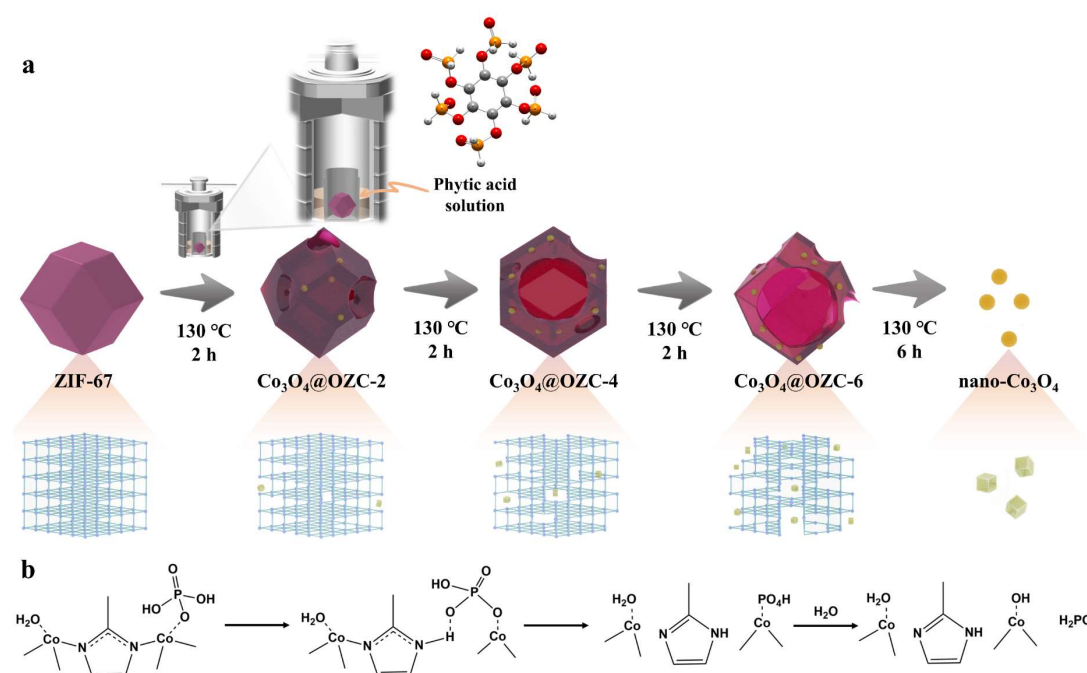
2.7 Preparation of polyurea composites

A typical preparation of polyurea composites containing 5 wt% as-prepared sample is illustrated as

follows. Briefly, the component A (50.00 g) was placed in a three-necked flask. Under nitrogen protection, 5.26 g of $\text{Co}_3\text{O}_4@\text{OZC-2}$ was slowly added into the component A and stirred at room temperature for 10 min. Subsequently, component B (50.00 g) was added to the above mixture with mechanical stirring for 10 min (400-600 revolutions per minute). Finally, the fully mixed two components were poured into a specific PTFE mold at room temperature for 3 days to prepare PUA elastomer $\text{PUA}/\text{Co}_3\text{O}_4@\text{OZC-2}$. Pure PUA, $\text{PUA}/\text{ZIF-67}$, $\text{PUA}/\text{Co}_3\text{O}_4@\text{OZC-4}$, $\text{PUA}/\text{Co}_3\text{O}_4@\text{OZC-6}$, and $\text{PUA}/\text{nano-Co}_3\text{O}_4$ samples were obtained by the above similar methods.

2.8 Characterization

Details of this section are in Supplementary Material.



Scheme 1. (a) Schematic illustration of synthesis process of open ZIF-67 cages (OZCs) by a gas-steamed metal–organic framework (GSM) approach. (b) The hypothesized formation mechanism for OZCs under acidic conditions.

3. Results and discussion

3.1. Synthesis and characterization

A series of $\text{Co}_3\text{O}_4@\text{OZC-x}$ were prepared according to the convenient GSM method using ZIF-67 as precursor and phytic acid as etchant. Morphology characterizations by scanning electron microscopy (SEM) and transmission electron microscopy (TEM) confirmed the successful preparation of these open-wall cage architectures (**Fig. 1a-c and Fig. 1e-g**). As expected, in the steaming condition derived from PA solution, obvious defects would occur on ZIF-67 while the main dodecahedron-like morphology are kept, resulting in unique open-wall architectures carrying “small pups”. Specifically, the as-prepared $\text{Co}_3\text{O}_4@\text{OZC-2}$ can maintain dodecahedron-like morphology similar to ZIF-67 (**Figure S3**). With the increase of etching time, the size and number of open holes gradually increase. When the etching time exceeds 6 h, the enlarged defect causes the collapse of the ZIF-67 crystal structure (**Fig. 1c and g**) and with a distinct element distribution of C, N, O, P and Co (**Fig. 1o, Figure S4, and Table S1**). **Fig. 1i-m** indicate that $\text{Co}_3\text{O}_4@\text{OZC-6}$ is composed of an amorphous shell layer derived from ZIF-67 and a highly crystalline 'small pups', i.e., tricobalt tetraoxide. Eventually, ZIF-67 is completely etched, leaving only the derived nano-cobaltosic oxide (**Fig. 1d and h**). Based on the elemental mapping images of nano- Co_3O_4 , only uniformly distributed Co and O elements can be observed (**Fig. 1n, Figure S5, and Table S2**), implying the dissociated cobalt ions are further oxidized to form cobaltosic oxide, which was further confirmed by the XRD patterns below.

Note that phytic acid molecules do not diffuse into the gas phase with water vapor at high temperature. Instead, it hydrolyzes to produce inositol phosphate with one to five phosphate groups along with the release of phosphoric acid. Thus, the defect formation for ZIF-67 is due to the protonation of the ligand by phosphoric acid, and the presumed mechanism is shown in **Scheme. 1b**. In order to validate

our conjecture, we chose low boiling point acids (such as phosphoric acid and glacial acetic acid), bases (such as ammonia), and compounds that decompose to produce alkaline substances (such as urea) as substitutes for phytic acid, respectively, and also achieved etching for ZIF-67 crystals to obtain similar structures. A series of experimental results were confirmed by SEM images (**Fig. 1p-s**). Under the condition of acid etching, the vaporized etchant randomly diffuses into the surface and skeleton of ZIF-67, which leads to the protonation of the basic ligand of ZIF-67. Furthermore, the released cobalt ions are accelerated oxidized by oxygen in a high temperature and confined environment, eventually forming cobalt tetraoxide nanoparticles. In the case of alkaline etching, the coordination bond between cobalt ion and ligand (Co-L) is weaker than that with OH⁻ hydrolyzed by ammonia gas (**Figure S6**), which makes ZIF-67 tend to dissociate and further form defects.³⁰

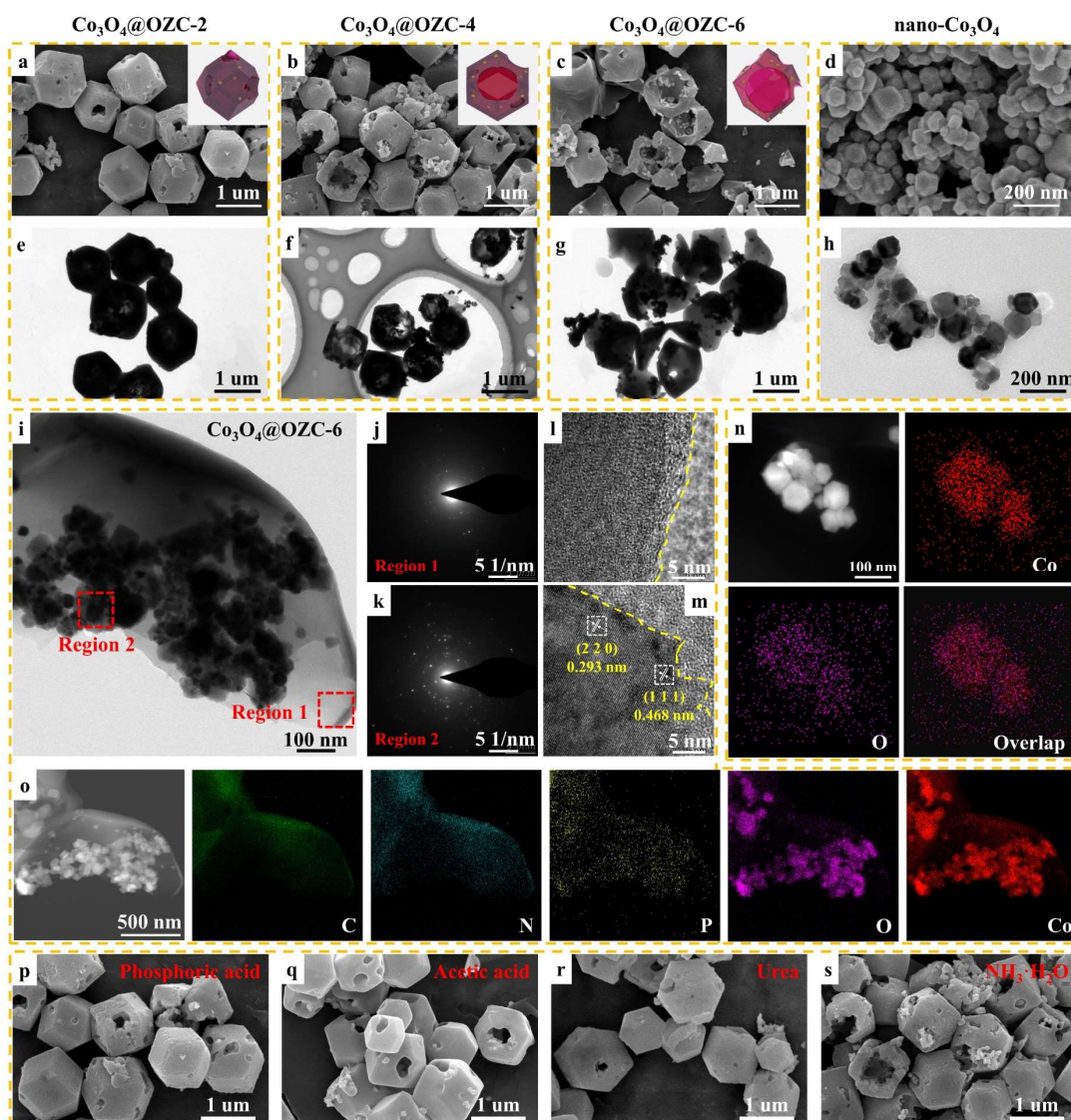


Fig. 1. (a, e) SEM and TEM image of $\text{Co}_3\text{O}_4@\text{OZC-2}$. (b, f) SEM and TEM image of $\text{Co}_3\text{O}_4@\text{OZC-4}$. (c, g) SEM and TEM image of $\text{Co}_3\text{O}_4@\text{OZC-6}$. (d, h) SEM and TEM image of nano- Co_3O_4 . (i) Enlarged TEM image, (j, k) selected area electron diffraction (SAED) pattern, (l, m) high-resolution TEM (HRTEM) images, (o) high angle annular dark field (HAADF) and corresponding elemental mapping images of $\text{Co}_3\text{O}_4@\text{OZC-6}$. (n) The HAADF and corresponding elemental mapping images of nano- Co_3O_4 . (p-s) Universality of the GSM approach for the preparation of OZCs. SEM images of OZCs obtained by selecting different etching agents. The inset in (a-c) show schematic diagram of the corresponding sample.

XRD pattern of $\text{Co}_3\text{O}_4@\text{OZC-2}$, $\text{Co}_3\text{O}_4@\text{OZC-4}$, and $\text{Co}_3\text{O}_4@\text{OZC-6}$ all retain the crystal structure of ZIF-67, but the peak intensity decreases gradually with the extension of etching time (**Fig. 2a**). This is attributed to destruction of the original crystal composition and the formation of enlarged channels after gas-steamed etching. Obviously, the characteristic peaks assigned to Co_3O_4 (*JCPDS No.42-1407*) were monitored in all etched ZIFs derivatives, and the phase belonging to ZIF-67 disappeared completely after etching for 12 h, which is consistent with the above TEM as well as energy dispersive spectroscopy (EDS) analysis.

The XPS spectra of as-prepared samples are presented in **Fig. 2b** in order to explore their elemental composition. The signal peak of the nitrogen element gradually decreases until it disappears primarily due to the dissociation from the organic ligand in ZIF-67. However, the disassociated cobalt ions are retained in the form of oxides. Thus, the content of cobalt and oxygen gradually increases with etching time (**Table S3**). Interestingly, small amounts of P elements are observed within the $\text{Co}_3\text{O}_4@\text{OZC-x}$ system. This may be attributed to the combination of phosphoric acid remaining in the pores with ligands or cobalt ions.

The BET results shed light on the structure differences of as-prepared samples after gas-steamed etching (**Fig. 2c-g**). The N_2 absorption-desorption isotherms of $\text{Co}_3\text{O}_4@\text{OZC-x}$ all have a hysteresis loop at P/P_0 of 0.4–0.8, which indicates that $\text{Co}_3\text{O}_4@\text{OZC-x}$ contain a large number of mesoporous. Specifically, the main pore diameter distribution of $\text{Co}_3\text{O}_4@\text{OZC-x}$ (2, 4 and 6) is above 2 nm (**Table S4**), indicating that the original ZIF-67 micropores have basically achieved reaming. However, part of micropores can still be observed in $\text{Co}_3\text{O}_4@\text{OZC-2}$, which are inherited from the ZIF-67. Moreover, the prolongation of etching time causes the disappearance of micropores in $\text{Co}_3\text{O}_4@\text{OZC-2}$, accompanied

by the gradual enlargement of mesopores and the appearance of macropores (**Figure S7**). This is also consistent with presented SEM and TEM images. Additionally, the specific surface area of the samples also presents a decreasing trend with the increasing of etching time (**Table S4**), all of which are lower than that of primitive ZIF-67 ($S_{\text{BET}} = 1668.2 \text{ m}^2/\text{g}$). This is caused by the loss of micropores and the formation of enlarged channels. However, $\text{Co}_3\text{O}_4@\text{OZC-x}$ can still maintain a high specific surface area, especially $\text{Co}_3\text{O}_4@\text{OZC-2}$, due to its unique framework structure of both micropores and mesopores under light etching. After 12 hours of gas-steamed etching, the specific surface area of nano- Co_3O_4 ($S_{\text{BET}} = 65.5 \text{ m}^2/\text{g}$) is obviously decreased compared with $\text{Co}_3\text{O}_4@\text{OZC-x}$, which is mainly attributed to the complete elimination of the ZIF-67-derived framework leaving only the solid Co_3O_4 .

Thermogravimetric analysis (TGA) was first employed to shed light on thermostability and flame retardant potential of samples (**Fig. 2h**). $\text{Co}_3\text{O}_4@\text{OZC-x}$ inherit the excellent thermal stability of ZIF-67, and their initial decomposition temperatures ($T_{5\%}$) are all increased, while the maximum thermal decomposition temperatures (T_{max}) are moved forward. This is ascribed to the disruption of the regular crystal structure of ZIF-67. Theoretically the proper early decomposition of the FRs helps to promote the early charring of the polymer matrix³¹. In detail, the mass loss of $\text{Co}_3\text{O}_4@\text{OZC-x}$ may be summarized in two stages (**Fig. 2i and Table S5**). The differences in thermal stability properties of the three may be accounted for by variations in crystal structure and composition. The $\text{Co}_3\text{O}_4@\text{OZC-2}$ exhibits excellent thermal stability because it preserves the crystal structure of ZIF-67 to the greatest extent while having fewer defects. Note that the residual char of $\text{Co}_3\text{O}_4@\text{OZC-x}$ is significantly higher than that of ZIF-67, which is inseparable from the improved catalytic activity, proper rejection of flammable ligands, and the content of highly thermally stable cobalt oxides.

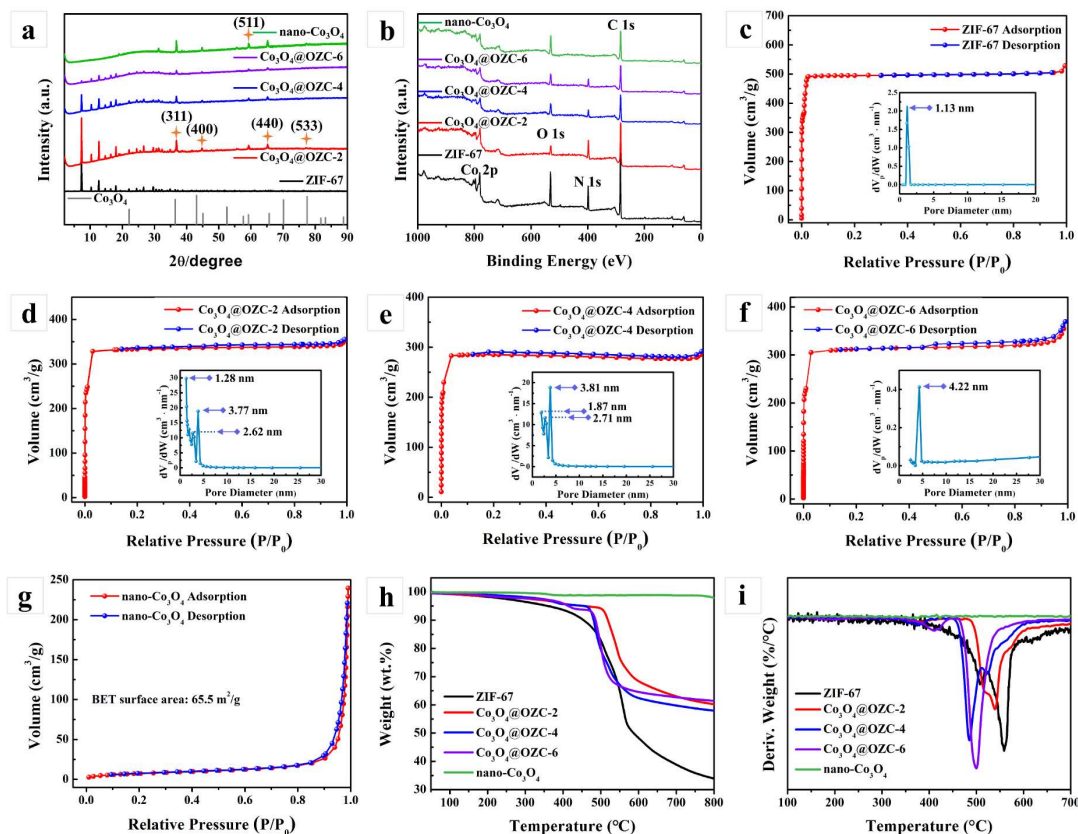


Fig. 2. (a, b) XRD pattern and XPS survey spectra for ZIF-67, $\text{Co}_3\text{O}_4@\text{OZC}-x$, and nano- Co_3O_4 . (c-g) Nitrogen sorption isotherms for ZIF-67, $\text{Co}_3\text{O}_4@\text{OZC}-x$, and nano- Co_3O_4 . The inset in (c-f) show pore diameter distribution of corresponding sample. (h and i) TGA profiles and DTG profiles of the products under nitrogen.

3.2. Thermal behavior and fire safety of the hybrids in PUA composites

The OZCs-based fillers all improve the glass transition temperature (T_g) for the PUA composites (**Figure S8**). Compared with the smooth ZIF-67, OZCs with passivated edges and corners are more conducive to full contact with polymer matrix and achieve stronger interfacial adhesion.^{32, 33} In addition, the surface of OZCs containing defects can provide more interfacial interaction energy. Compared with the original ZIF-67, the defective OZCs can obtain greater surface adhesion strength.³⁴ However, the thermally conductive Co_3O_4 nanoparticles partially counteracts the interaction of OZCs with polyurea

molecular chains, leading to a decrease in the T_g of the composite, especially for PUA/Co₃O₄@OZC-6. Just these comprehensive factors lead to the change of glass transition temperature of PUA composites. The introduction of flame retardant fillers significantly promotes the pyrolytic behavior of PUA matrix due to the catalytic effect of the fillers. PUA/Co₃O₄@OZC-x have similar decomposition behavior (**Fig. 3a and b**), with similar $T_{5\%}$ as well as T_{max} (**Table S6**). Specifically, mass loss near 380 °C may result from ligand decomposition of fillers. Subsequently, the weight loss rate increases sharply due to the decomposition of the PUA matrix. Another drastic mass loss is presented after 650 °C, which can be attributed to the further decomposition of the cobalt-doped carbon compound to form a more stable carbon residue. In general, appropriate early decomposition can promote the formation of char for flame retardant polymer composites, with Co₃O₄@OZC-2 the most obvious effect, Co₃O₄@OZC-4 the second, Co₃O₄@OZC-6 the worst. This is attributed to the low catalytic activity of Co₃O₄, which impairs the catalytic efficiency of OZCs.

The fire hazards of PUA composites involving high release of heat, smoke, and poisonous gases (such as carbon monoxide). Once exposed to the fire environment, fire safety problems will occur, which greatly limits the application of PUA. Especially, inhibiting the release of smoke and toxic gases from PUA composites is of more practical significance for the rescue and escape of personnel.³⁵ Flame retardancy of PUA composites was first evaluated by LOI tests (**Table S7**). Pure PUA has a LOI value of only 17.8%. For PUA composites blended with Co₃O₄@OZC-x, their LOI values are increased in different degrees. And the values of PUA compounded with Co₃O₄@OZC-2, Co₃O₄@OZC-4, and Co₃O₄@OZC-6 were 21.2%, 20.8%, and 20.1%, respectively. However, nano-Co₃O₄ did not significantly improve the flame retardant properties of PUA composites, which may be attributed to its low specific

surface area that severely restrict its catalytic charring efficiency for the matrix (**Table S4**).

The flame retardancy as well as the combustion behavior of PUA composites were further evaluated by Cone according to the ISO 5660 protocol. The pristine PUA exhibits the highest pHRR value at 810 kW/m². While the pHRR values of all PUA/Co₃O₄@OZC-x composites are decreased significantly compared with pure PUA, among which PUA/Co₃O₄@OZC-2 shows the lowest pHRR value (506 kW/m²) and THR value (70.9 MJ/m²) (**Fig. 3c and d**). The hierarchical pores and high-exposure transition metals can effectively promote catalytic charring of the cracked products, which in turn blocks the flow of heat and combustibles. PUA/ZIF-67 composite shows better inhibition than PUA/Co₃O₄@OZC-6 for the heat of combustion, which is mainly because the formed Co₃O₄ nanoparticles sacrifice the catalytic efficiency of OZCs.

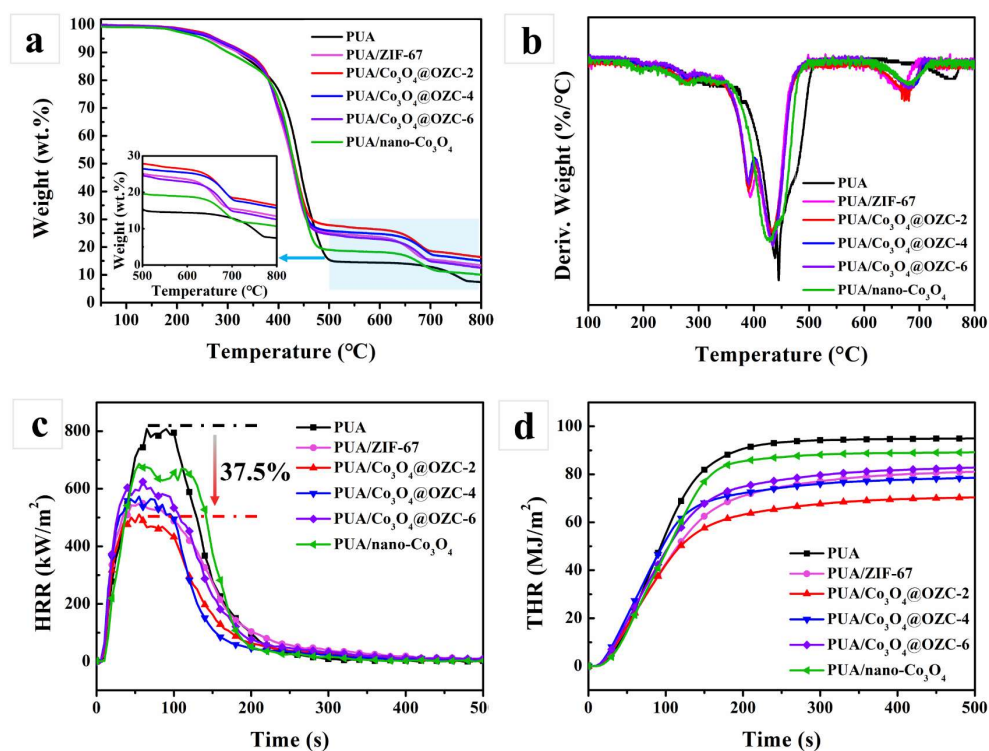


Fig. 3. (a) TGA and (b) DTG profiles of PUA and its composites under nitrogen. (c) heat release rate (HRR) and (d) total heat release curves of PUA and its composites.

Flame retardancy index (FRI) is a dimensionless general index used to evaluate the flame retardancy of nanocomposites based on Cone data.³⁶ And the specific calculation method is shown in **Eq. (1)**. The higher the FRI value, the lower the fire risk, indicating that the longer it takes for the material to reach flashover and cause the fire to develop fully. The FRI value of PUA/Co₃O₄@OZC-2 is the highest (1.836), which once again shows that high exposed active sites are more conducive to matrix charring, thus inhibiting the combustion heat.

$$FRI = \frac{\left(THR \times \frac{\text{maximum HRR}}{\text{time to maximum HRR}}\right)_{\text{pure polymer}}}{\left(THR \times \frac{\text{maximum HRR}}{\text{time to maximum HRR}}\right)_{\text{composite}}} \quad (1)$$

The peak of smoke production rate (pSPR) and TSP of PUA/Co₃O₄@OZC-2 composite are significantly reduced by 29.7% and 40.4%, respectively, relative to pure PUA. Moreover, the SPR and TSP of PUA/Co₃O₄@OZC-2 are significantly lower than those of PUA/ZIF-67, which suggests that the hierarchical pores are beneficial to absorb and catalysis the smoke particles and pyrolytic volatiles (**Fig. 4a and b**).²⁴ Smoke factor (SF), which is the product of HRR and TSR, is usually employed to comprehensively evaluate the smoke generation condition of the polymer during combustion.³⁷ The SF curves are described in **Fig. 4c**. The SF peak of pure PUA is about 383.6 MW/m², while the SF peak values of PUA/ZIF-67 composites are much lower than that of pure PUA but higher than PUA/Co₃O₄@OZC-2. In detail, the SF peak value of PUA/Co₃O₄@OZC-2 decreases by 39.2% compared with neat PUA. PUA/Co₃O₄@OZC-2 shows the most excellent smoke capture capability compared with PUA/Co₃O₄@OZC-4 and PUA/Co₃O₄@OZC-6, which may be attributed to the optimal matching between the pore characteristics of Co₃O₄@OZC-2 and the size of the smoke particles decomposed by the PUA matrix. This integrated microporous and mesoporous structure is more advantageous for the adsorption of smoke and toxic gases. Moreover, the adsorption capacity of Co₃O₄@OZC-4 is slightly

higher to that of ZIF-67 with microporous structure. On the one hand, the oversized mesopore size does not match the size of the smoke particles.²⁵ On the other hand, the increase in larger pores comes at the expense of more micropores, while the larger pores themselves have no significant effect on the adsorption of smoke particles.

As consistent with the above analysis. The introduction of $\text{Co}_3\text{O}_4@\text{OZC-2}$ is the most obvious for reducing the release of CO and CO_2 from the PUA composite (**Fig. 4d and e**). One is that the flame-retardant filler promotes the formation of condensed phase char layer.³⁸ Besides, CO is adsorbed on the surface of the metal oxide derived from as-prepared flame retardant fillers reducing its oxidation potential and further facilitating the reaction with oxygen to form CO_2 .³⁹ The CO and CO_2 release profiles also reaffirm that the hierarchical porous and open-walled catalytic structure has more significant advantages for the inhibition of smoke and toxic gas release.

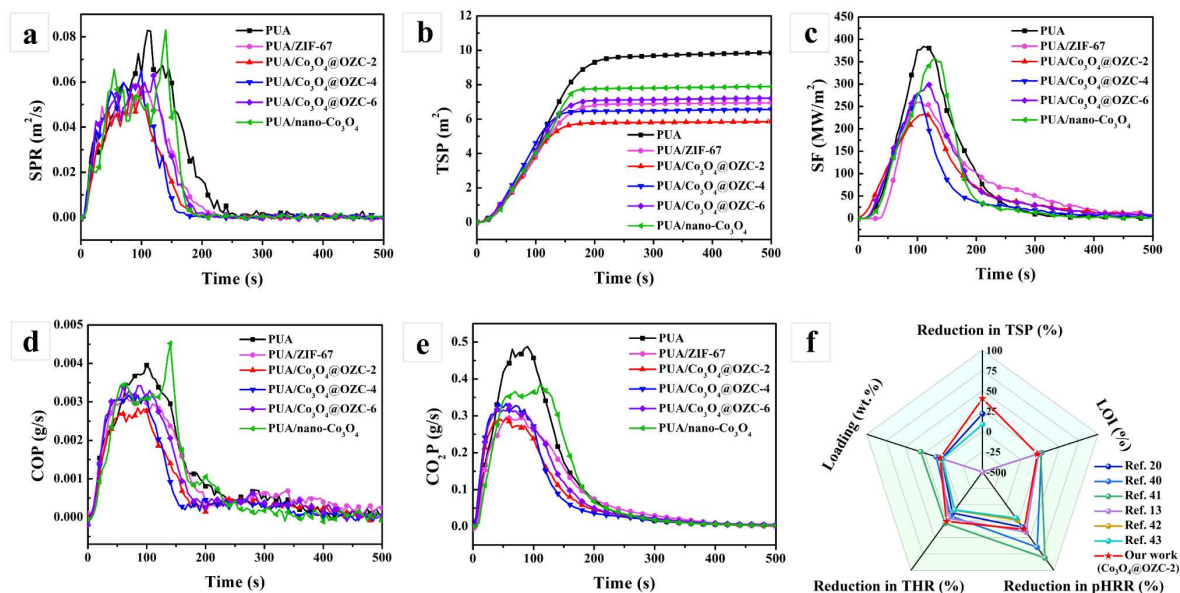


Fig. 4. (a) Smoke production rate, (b) total smoke production, (c) smoke factor, (d) carbon monoxide production (COP), and (e) carbon dioxide production (CO_2P) curves of PUA and its composites. (f) comparison of flame retardants used in PUA or TPU composites in the literature.

The char-forming properties of PUA composites are visually depicted by the post-combustion char residues (**Table S7**). PUA integrated with $\text{Co}_3\text{O}_4@\text{OZC-2}$ has the highest residual char mass (13.2%), while that of pure PUA is only 3.9%. The char residue of PUA/ZIF-67 is similar to that of PUA/ $\text{Co}_3\text{O}_4@\text{OZC-4}$ and PUA/ $\text{Co}_3\text{O}_4@\text{OZC-6}$, which also shows the damage of Co_3O_4 to the catalytic char formation performance of OZCs system again. From the above results, it can be seen that PUA/ $\text{Co}_3\text{O}_4@\text{OZC-2}$ has superior fire safety performance than other PUA composites. **Fig. 4f** and **Table 1** provide a comparison of high-performance FRs for polyurea or thermoplastic urethane (TPU) in the last years. The $\text{Co}_3\text{O}_4@\text{OZC-2}$ in this work displays comprehensive fire safety performance at low dose, especially for the suppression of smoke and toxic gases.

Table 1. Combustion properties of TPU/PUA composites in the literature.

Flame retardant	Loading (wt%)	LOI (%)	Reduction in pHRR (%)	Reduction in THR (%)	Reduction in TSP (%)	References
NiMoO ₄ @Co-Ni LDH	3	-	34.4%	12.7%	21.7%	20
Ammonium polyphosphate & Chitosan (1:1)	10	26.6	64.8%	≈17.0%	-	40
Ammonium polyphosphate / Montmorillonite & Charring-foaming agent (5:1)	30	25.6	81.2%	28.3%	-	41
TPP-loaded m-CBC@LDH	5	22.6	41.6%	20.6%	-465.6%	13
ZnO/MOF/PZS	3	-	23.5%	8.4%	-	42
h-BN@SiO ₂ @PA	2	-	20.4%	8.0%	8.6%	43
Our Work (Co₃O₄@OZC-2)	5	21.2	37.5%	25.5%	40.4%	

3.3. Condensed-phase and gaseous-phase analysis of PUA composites

The characteristics of char residues for PUA composites after Cone tests were further evaluated by digital camera and SEM (**Fig. 5a-f**). A large number of holes exist the post-burn char residue of pure PUA, and obvious pores and cracks can be observed under microscopy. The introduction of flame retardant fillers significantly improved the residual char yield and enhanced the denseness of the char layer. This is beneficial in blocking the diffusion of heat and combustibles and slowing down the combustion progress of PUA matrix.^{44, 45} Subsequently, the char residue of polyurea and its composites

after the Cone test was further analyzed by physical adsorption. The specific surface area of all residual char is very low, and there is no obvious change (**Table S8**). However, the pore diameter distribution of the residual char of the OZCs-modified polyurea composites is significantly reduced, which may be related to the formation of a dense char layers.

Raman spectroscopy was employed to characterize residual char, which is considered an efficacious characterization technique, particularly for carbonaceous materials. As revealed by the Raman spectra, the peak integral ratios (I_D/I_G) of the disorder-induced D band to the G band reflecting graphite degree. The high graphitization char layer has more significant advantages in terms of oxidation resistance, and the improved stability for the char layer can effectively restrain fire transfer.⁴⁶ The I_D/I_G value of PUA/Co₃O₄@OZC-2 was lower than that of PUA/Co₃O₄@OZC-4, while the I_D/I_G value of PUA/ZIF-67 was higher than that of PUA/Co₃O₄@OZC-4, but slightly lower than that of PUA/Co₃O₄@OZC-6 (**Fig. 5a-f**). The decrease in I_D/I_G values is evidence of enhanced graphitization and fewer structural defects within the char layer derived from PUA composites.⁴⁷ Additionally, **Figure S9** presents the phase and composition of the residual char from post-Cone test of PUA composites. The residual char of PUA composites shows characteristic peaks of cobalt oxides, namely CoO (*JCPDS No. 43-1044*) and Co₃O₄ (*JCPDS No. 43-1003*), except for the pure PUA.¹³ Char residue doped with cobalt oxide is beneficial to improve the thermal stability of char layer.⁴⁸

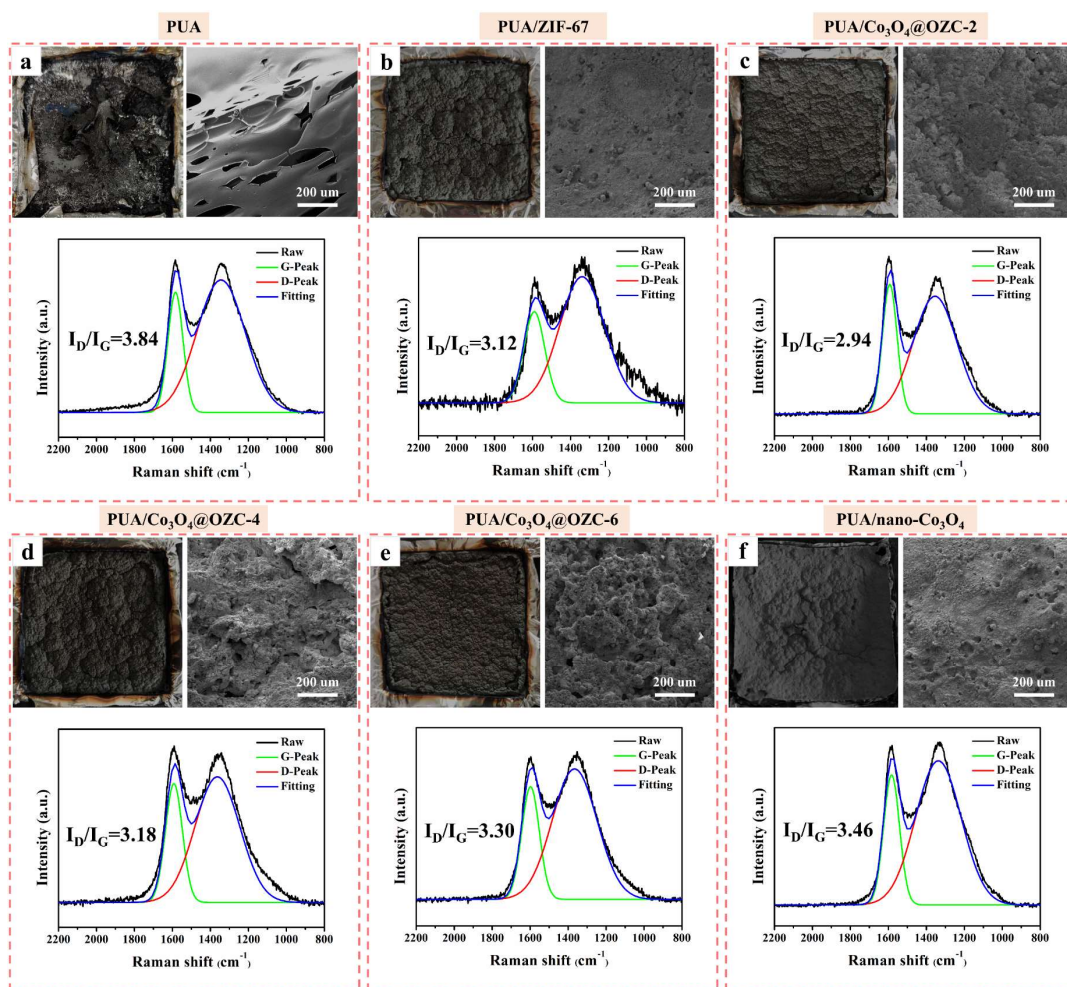


Fig. 5. Digital photographs, SEM images, and Raman spectra of char residues after Cone tests from (a) PUA, (b) PUA/ZIF-67, (c) PUA/Co₃O₄@OZC-2, (d) PUA/Co₃O₄@OZC-4, (e) PUA/Co₃O₄@OZC-6, and (f) PUA/nano-Co₃O₄.

TG-FTIR technology was employed to study the gaseous pyrolysis products and their evolution during the thermal degradation of pure PUA and its composites. As shown in **Fig. 6a** and **6b**, the 3D TG-FTIR spectra intuitively shows that the Co₃O₄@OZC-2 could significantly inhibit the release of gas products from the decomposition of PUA matrix. The total pyrolysis gaseous intensity versus time curves (Gram-Schmidt curves) of PUA and PUA/Co₃O₄@OZC-2 are presented in **Fig. 6c**. Obviously, the total release absorbance of the cleavage products from PUA/Co₃O₄@OZC-2 is significantly lower than that

of neat PUA. The gaseous phase decomposition products from PUA/Co₃O₄@OZC-2 at the initial decomposition temperature are significantly stronger than pure PUA (**Fig. 6d**). This is mainly attributed to the fillers accelerate the pre-emptive decomposition of the polyurea matrix, accompanied by a stronger signal of gaseous release. And corresponding peaks in PUA and PUA composites appear at 2933, 2352, 2262, 1743, 1243, 1153, and 890 cm⁻¹, assigned to C–H, CO₂, CO, C=O, C–O–C, O–C=O, and N–H, respectively.⁴⁹ However, at the maximum thermal decomposition temperature, all gaseous products except CO₂ from PUA/Co₃O₄@OZC-2 are significantly reduced compared to pure PUA (**Fig. 6e**). This is inseparable from the excellent char formation performance and oxygen catalytic capacity of the filler. This phenomenon can also be uncovered in the evolution pattern of the characteristic cleavage gases versus time. More detailed clues are provided through the release curves for esters, ethers, carbonyl compound, and hydrocarbons, which are identified as flame-supporting fuels (**Fig. 6f and i-k**).⁵⁰ Clearly, the combustibles produced by the decomposition of PUA composites are significantly suppressed relative to pure PUA. Moreover, the release of CO₂ from PUA composites is significantly elevated, while the release of CO is significantly inhibited (**Fig. 6g and h**), which again prove the oxygen-catalytic property of Co₃O₄@OZC-2.⁵¹ The analysis reveal that Co₃O₄@OZC-2 also functions in the gas phase based on excellent physical and chemical adsorption capabilities from hierarchical pore, oxygen catalysis, and catalytic charring.

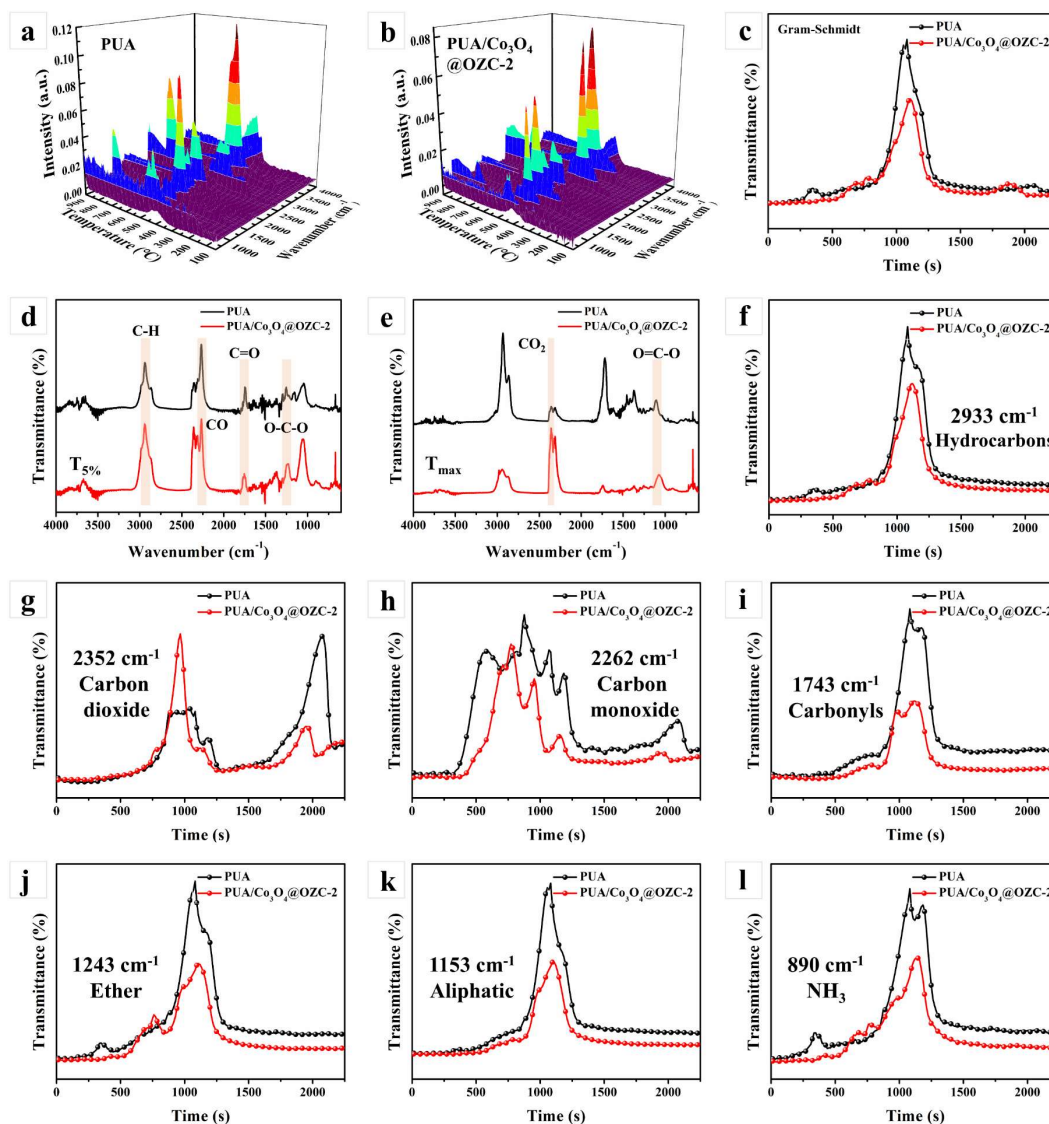
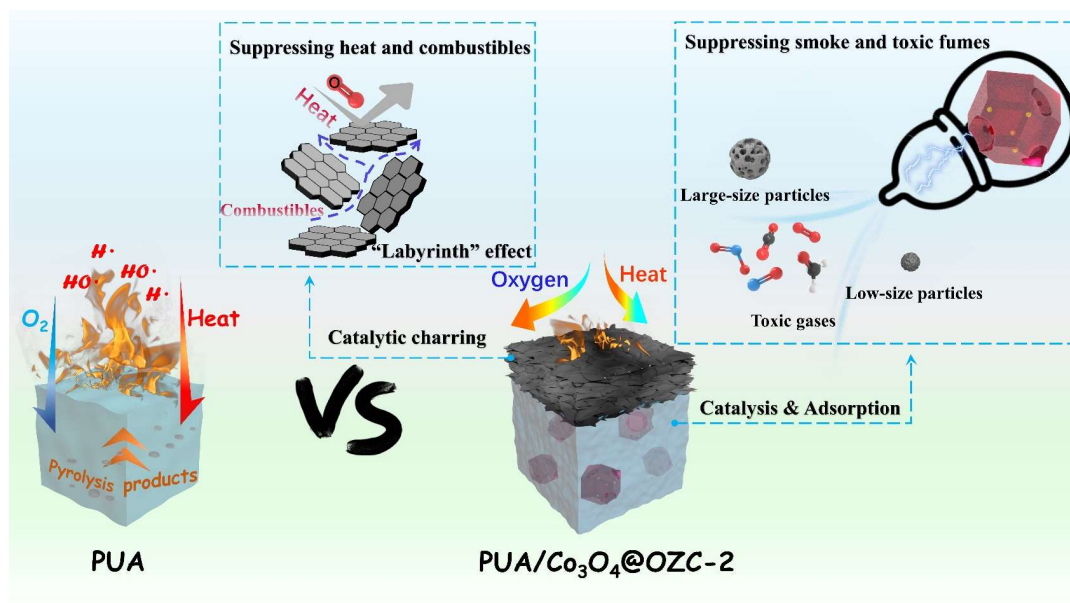


Fig. 6. (a and b) 3D TG-FTIR spectra, (c) Gram-Schmidt, (d and e) FT-IR spectra of pyrolysis products at the $T_{5\%}$ and T_{max} , (f) hydrocarbons, (g) carbon dioxide, (h) carbon monoxide, (i) carbonyls, (j) ether, (k) aliphatic, and (l) NH_3 release profiles for PUA and $\text{PUA}/\text{Co}_3\text{O}_4@\text{OZC-2}$.

3.4. Analysis of flame-retardant mechanism

Based on the above analysis, $\text{Co}_3\text{O}_4@\text{OZC-2}$ can effectively promote the adsorption of pyrolytic volatiles and catalytic char-formation of the matrix, and the speculated flame retardant mechanism is summarized in **Scheme 2**. On the one hand, $\text{Co}_3\text{O}_4@\text{OZC-2}$ contains transition metal elements with

catalytic effect, and its open-wall structure and high specific surface area expose more active sites, which enhances the formation of compact char layer.^{52, 53} On the other hand, $\text{Co}_3\text{O}_4@\text{OZC-2}$ features a hierarchical pore structure that slows down the release of volatiles during the decomposition of the matrix. Because of this unique structure, toxic gases and smoke particles are easily trapped by the cage through physical and chemical adsorption, and they have to go through a more complex pathway than usual, the so-called "labyrinth" effect.^{24, 25} Impressively, catalytic structures with both mesopores and micropores are more effective than solely micropore catalytic structures for smoke and toxic gas inhibition, as mesoporous structures can capture large size smoke particles more efficiently. However, out-of-size mesoporous structures may impair the adsorption capacity for smoke. It is through the above multi-synergistic effect that $\text{Co}_3\text{O}_4@\text{OZC-2}$ makes the flame retardancy, especially smoke suppression, of PUA composites significantly improved.



Scheme 2. Schematic of flame-retardant mechanism for PUA/ $\text{Co}_3\text{O}_4@\text{OZC-2}$ composite.

3.5. Dispersion behavior and mechanical properties of the hybrids in PUA composites

The dispersion of FRs in polymer matrix is a crucial factor affecting the mechanical properties and

fire safety of composites.⁵⁴ The pure PUA presents a smooth fracture morphology (**Figure S10**), while the PUA composites blended with a series of fillers all show the fairly rough morphologies with the large-crinkled (**Fig.7 a-d and Figure S11**). The altered fracture mode of PUA composites is caused by the enhanced interaction forces between the additives and the matrix. Moreover, the increased fracture propagation path and area leads to energy dissipation and enhanced toughness.^{25, 29} **Fig. 7 a-d** (part of PUA composites cross-section are enlarged and marked with yellow line) preliminarily confirm the uniform dispersion of the filler without significant agglomeration.

In contrast to PUA/ZIF-67, the tensile strength and elongation at break of PUA/Co₃O₄@OZC-x are improved in different degrees, respectively (**Fig. 7e and f**). This is mainly due to the fact that Co₃O₄@OZC-x with open structure is embedded in the PUA matrix, which can bear and disperse the stress in time, thus absorbing more energy and improving the tensile strength of the composite.²⁹ However, if the OZCs carry too much cobalt tetroxide nanoparticles (Co₃O₄@OZC-6), this is detrimental to the improvement of mechanical properties. Compared with pure PUA, the mechanical properties of PUA/Co₃O₄@OZC-2 and PUA/Co₃O₄@OZC-4 composites are not drastically reduced. The acceptable mechanical property is mainly ascribed to the better interfacial compatibility between the filler and polyurea matrix. The open structure of OZCs enhances the interfacial interaction between the filler and polymer chains, and OZCs and Co₃O₄ cooperate to play the enhancement mechanism of dimension dislocation as well.^{55, 56} Notably, the blended polyurea composites with nano-Co₃O₄ showed the worst mechanical properties (**Table S9**). On the one hand, this is due to the complete removal of ligands during the evolution of ZIF-67 into nano-Co₃O₄, while the ligands facilitate the enhancement of the compatibility between the filler and the polyurea matrix. On the other hand, the agglomeration problem

of nano- Co_3O_4 affects the continuity of the matrix and forms many stress concentration points, which can easily trigger the generation of cracks.⁷ In addition, the Shore hardness of PUA composites is slightly improved due to the introduction of rigid flame retardant filler (Table S10).

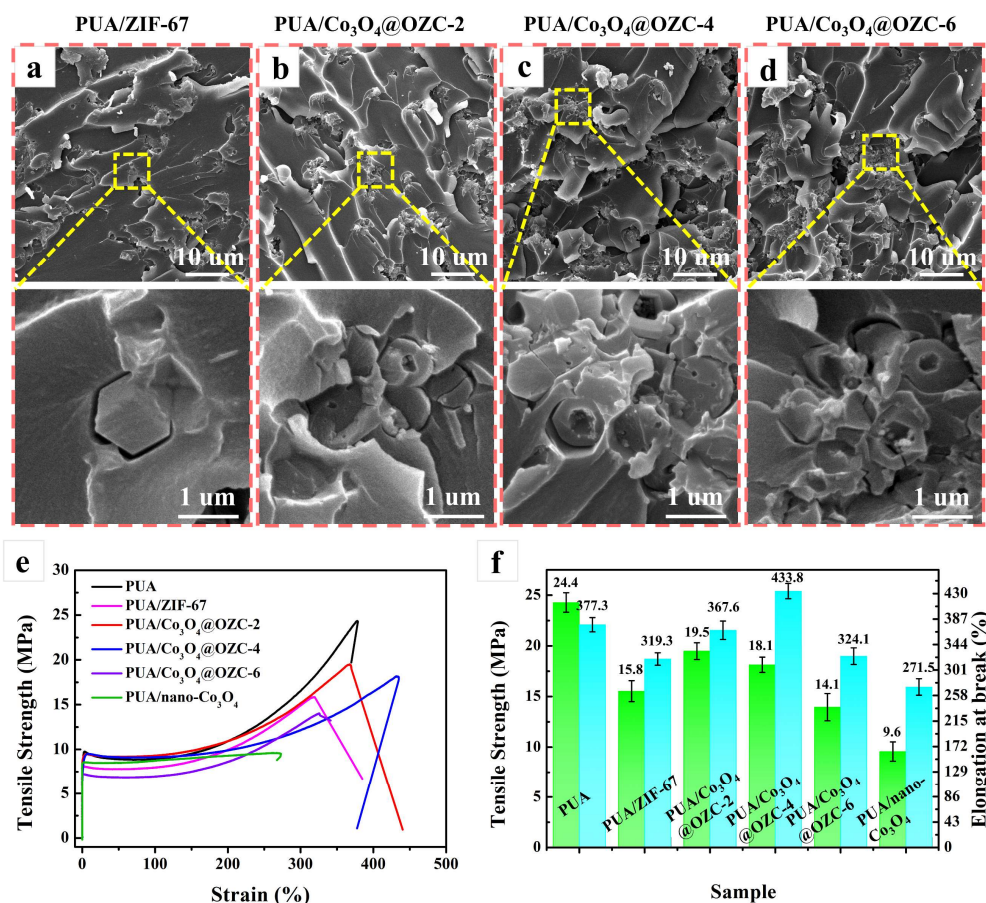


Fig. 7. (a–d) SEM images and enlarged SEM images of the fractured surface for PUA/ZIF-67, PUA/ Co_3O_4 @OZC-2, PUA/ Co_3O_4 @OZC-4, and PUA/ Co_3O_4 @OZC-6 composites. (e) stress–strain profiles and (f) histogram of tensile strength as well as elongation at break of PUA and its composites.

4. Conclusion

In the work, we have developed a gas-steamed ZIFs route, which abandoned the traditional environmentally unfriendly wet chemical synthesis method for the preparation of open mesoporous ZIF cages with certain universality. The OZCs with dominant mesoporous pores play a better role for the

capture of smoke toxins than microporous ZIF-67. Evaluation of a series of OZCs based on combustion, thermal and mechanical tests confirmed that $\text{Co}_3\text{O}_4@\text{OZC-2}$ has the best comprehensive performance. Specifically, the pHRR, THR, TSP of PUA composites mixed with 5 wt % $\text{Co}_3\text{O}_4@\text{OZC-2}$ were reduced by 37.5%, 25.5%, and 40.4%, respectively, compared to pure PUA. The enhanced activity originates from its unique open-wall structure and mesopore-dominated hierarchical pores, which can adsorb and catalyze cracking products more effectively. Unfortunately, the OZCs prepared by this strategy suffer from the inevitable problem of carrying Co_3O_4 nanoparticles, and the process of enlarging pore size for OZCs is accompanied by the formation of more Co_3O_4 together with the sacrifice of specific surface area. This is not conducive to the efficient catalytic and trapping capability of OZCs, so it is also the main factor leading to the degradation of $\text{Co}_3\text{O}_4@\text{OZC-4}$ and $\text{Co}_3\text{O}_4@\text{OZC-6}$ performance. Meanwhile, the tensile strength and elongation at break of PUA/ $\text{Co}_3\text{O}_4@\text{OZC-2}$ are significantly enhanced compared with PUA/ZIF-67, attributed to the open structure that enhance the filler-matrix interactions. This gas-steamed MOFs strategy will open an avenue to design functional nanostructures for possible fire safety and other applications.

ASSOCIATED CONTENT

Supporting Information.

The Supporting Information is available free of charge at XXXXXXXXXXXXXXXX.

Experimental section (Materials, Preparation of samples, and Characterization); TEM images, SEM images, EDS spectra, TEM-EDS data, XPS data, pore diameter distribution, BET surface area data, and TGA data of samples; Fractured surface, Shore hardness data, tensile data, DSC curves, TGA data, LOI data, and Cone data of PUA and its composites; XRD spectra and BET surface area data of char residues after Cone tests from PUA and its composites. (.pdf)

Abbreviations

ZIF-67, Zeolitic imidazolate framework-67; $\text{Co}_3\text{O}_4@OZC-2$, $\text{Co}_3\text{O}_4@open$ ZIF-67 cages-2; $\text{Co}_3\text{O}_4@OZC-4$, $\text{Co}_3\text{O}_4@open$ ZIF-67 cages-4; $\text{Co}_3\text{O}_4@OZC-6$, $\text{Co}_3\text{O}_4@open$ ZIF-67 cages-6; $\text{Co}_3\text{O}_4@OZC-H_3PO_4$, $\text{Co}_3\text{O}_4@open$ ZIF-67 cages with phosphoric acid as etchant; $\text{Co}_3\text{O}_4@OZC-CH_3COOH$, $\text{Co}_3\text{O}_4@open$ ZIF-67 cages with acetic acid as etchant; $\text{Co}_3\text{O}_4@OZC-NH_3 \cdot xH_2O$, $\text{Co}_3\text{O}_4@open$ ZIF-67 cages with ammonia solution as etchant; $\text{Co}_3\text{O}_4@OZC-(NH_2)_2CO$, $\text{Co}_3\text{O}_4@open$ ZIF-67 cages with urea as etchant

AUTHOR INFORMATION

Corresponding Author

Ye-Tang Pan - *National Engineering Research Center of Flame Retardant Materials, School of Materials Science & Engineering, Beijing Institute of Technology, Beijing 100081, PR China; orcid.org/0000-0002-2850-5129; Email: pyt@bit.edu.cn*

Jiyu He - *National Engineering Research Center of Flame Retardant Materials, School of Materials Science & Engineering, Beijing Institute of Technology, Beijing 100081, PR China*

Email: hejiyu@bit.edu.cn

Authors

Kunpeng Song - *National Engineering Research Center of Flame Retardant Materials, School of Materials Science & Engineering, Beijing Institute of Technology, Beijing 100081, PR China*

Xue Bi - *National Engineering Research Center of Flame Retardant Materials, School of Materials Science & Engineering, Beijing Institute of Technology, Beijing 100081, PR China*

Chuang Yu - *National Engineering Research Center of Flame Retardant Materials, School of Materials Science & Engineering, Beijing Institute of Technology, Beijing 100081, PR China*

Henri Vahabi - *Université de Lorraine, CentraleSupélec, LMOPS, F-57000 Metz, France*

Vera Realinho - *Poly2 Group, Department of Materials Science and Engineering, School of Industrial, Aerospace and Audiovisual Engineering of Terrassa, Universitat Politècnica de Catalunya (UPC BarcelonaTech), C/ de Colom, 11, 08222 Terrassa, Spain*

Rongjie Yang - *National Engineering Research Center of Flame Retardant Materials, School of*

Materials Science & Engineering, Beijing Institute of Technology, Beijing 100081, PR China

CRedit authorship contribution statement

Kunpeng Song: Methodology, Investigation, Writing—original draft, Formal analysis. **Xue Bi and**

Chuang Yu: Data curation, Investigation. **Henri Vahabi and Vera Realinho:** Data curation,

Supervision. **Ye-Tang Pan:** Conceptualization, Funding acquisition, Writing—review & editing. **Jiyu He:**

Funding acquisition, Writing—review & editing. **Rongjie Yang:** Methodology, Supervision.

Declaration of Competing Interest

The authors declare that they have no known competing financial interests or personal relationships that could have appeared to influence the work reported in this paper.

Data availability

No data was used for the research described in the article.

Acknowledgement

This work was supported by the National Natural Science Foundation of China (no. 22005029 and 22375023) and the BIT Research and Innovation Promoting Project (Grant No. 2023YCX041). The authors extend their gratitude to Mr. Mengyun Cao from Shiyanjia Lab (www.shiyanjia.com) for providing invaluable assistance with the TME testing. The carbon-coated formvar film was provided by Zhongjingkeyi (Beijing) Film Technology Co., Ltd.

References

- (1) Kumar, N.; Gupta, P. K.; Khilari, S.; Ranganath, K. V. S. Synthesis, characterization and catalytic application of functionalized polyureas. *J. Polym. Res.* **2023**, *30* (3), 104. DOI: 10.1007/s10965-023-03492-1.
- (2) Wang, M.; Xie, Q.; Pan, J.; Ma, C.; Zhang, G. Strong yet tough cross-linked oligosiloxane elastomer with impact-resistant and antifouling properties. *Chem. Eng. J.* **2023**, *464*, 142769. DOI: <https://doi.org/10.1016/j.cej.2023.142769>.
- (3) Han, S.; Yang, F.; Li, Q.; Sui, G.; Kalimuldina, G.; Araby, S. Synergetic Effect of α -ZrP Nanosheets and Nitrogen-Based Flame Retardants on Thermoplastic Polyurethane. *ACS Appl. Mater. Inter.* **2023**, *15* (13), 17054-17069. DOI: 10.1021/acsami.2c20482.
- (4) Lu, J.-H.; Xu, Y.-J.; Chen, L.; Chen, J.-H.; He, J.-H.; Li, Z.; Li, S.-L.; Wang, Y.-Z. Facile fabrication of intrinsically fire-safety epoxy resin cured with phosphorus-containing transition metal complexes for flame retardation, smoke suppression, and latent curing behavior. *Chem. Eng. J.* **2022**, *442*, 136097. DOI: <https://doi.org/10.1016/j.cej.2022.136097>.
- (5) Wan, M.; Shi, C.; Qian, X.; Qin, Y.; Jing, J.; Che, H.; Ren, F.; Li, J.; Yu, B.; Zhou, K. Design of novel double-layer coated ammonium polyphosphate and its application in flame retardant thermoplastic polyurethanes. *Chem. Eng. J.* **2023**, *459*, 141448. DOI: <https://doi.org/10.1016/j.cej.2023.141448>.
- (6) Naik, A. D.; Bourbigot, S.; Bellayer, S.; Touati, N.; Ben Tayeb, K.; Vezin, H.; Fontaine, G. Salen Complexes as Fire Protective Agents for Thermoplastic Polyurethane: Deep Electron Paramagnetic Resonance Spectroscopy Investigation. *ACS Appl. Mater. Inter.* **2018**, *10* (29), 24860-24875. DOI: 10.1021/acsami.8b07323.
- (7) Sun, Y.; Yang, P.; Sun, W. Effects of kaolinite on thermal, mechanical, fire behavior and their mechanisms of intumescent flame-retardant polyurea. *Polym. Degrad. Stab.* **2022**, *197*, 109842. DOI: <https://doi.org/10.1016/j.polymdegradstab.2022.109842>.
- (8) Chen, D.; Qin, X.; Cao, X.; Wei, F.; Thummavichai, K.; Ola, O.; Wang, N.; Jiang, M.; Zhu, Y. Selective laser sintering of functionalized carbon nanotubes and inorganic fullerene-like tungsten disulfide reinforced polyamide 12 nanocomposites with excellent fire safety and mechanical properties. *J. Cleaner Prod.* **2023**, *401*, 136630. DOI: <https://doi.org/10.1016/j.jclepro.2023.136630>.
- (9) Zou, S.; Dang, L.; Li, Y.; Lan, S.; Zhu, D.; Li, L. Inorganic-organic dual modification of magnesium borate whisker by magnesium hydrate and dodecyl dihydrogen phosphate and its effect on the fire safety and mechanical properties of epoxy resin. *Appl. Surf. Sci.* **2022**, *589*, 153064. DOI: <https://doi.org/10.1016/j.apsusc.2022.153064>.
- (10) Song, K.; Pan, Y.-T.; Zhang, J.; Song, P.; He, J.; Wang, D.-Y.; Yang, R. Metal–Organic Frameworks–Based Flame-Retardant System for Epoxy Resin: A Review and Prospect. *Chem. Eng. J.* **2023**, *468*, 143653. DOI: <https://doi.org/10.1016/j.cej.2023.143653>.
- (11) Hou, Y.; Liu, L.; Qiu, S.; Zhou, X.; Gui, Z.; Hu, Y. DOPO-Modified Two-Dimensional Co-Based Metal–Organic Framework: Preparation and Application for Enhancing Fire Safety of Poly(lactic acid). *ACS Appl. Mater. Inter.* **2018**, *10* (9), 8274-8286. DOI: 10.1021/acsami.7b19395.

- (12) Zhou, X.; Qiu, S.; Mu, X.; Zhou, M.; Cai, W.; Song, L.; Xing, W.; Hu, Y. Polyphosphazenes-based flame retardants: A review. *Compos. Part B-Eng.* **2020**, *202*, 108397. DOI: <https://doi.org/10.1016/j.compositesb.2020.108397>.
- (13) Song, K.; Zhang, H.; Pan, Y.-T.; Ur Rehman, Z.; He, J.; Wang, D.-Y.; Yang, R. Metal-organic framework-derived bird's nest-like capsules for phosphorous small molecules towards flame retardant polyurea composites. *J. Colloid Interface Sci.* **2023**, *643*, 489-501. DOI: <https://doi.org/10.1016/j.jcis.2023.04.047>.
- (14) Luo, J.; Shi, X.; Chen, P.; Han, K.; Li, X.; Cao, X.; Wang, Z. L. Strong and flame-retardant wood-based triboelectric nanogenerators toward self-powered building fire protection. *Mater. Today Phys.* **2022**, *27*, 100798. DOI: <https://doi.org/10.1016/j.mtphys.2022.100798>.
- (15) Zou, B.; Qiu, S.; Jia, P.; Jiang, X.; Song, L.; Hu, Y. Photothermal and fire-safe epoxy/black phosphorene composites: Molecular structure analysis of sutured char. *Appl. Surf. Sci.* **2022**, *605*, 154848. DOI: <https://doi.org/10.1016/j.apsusc.2022.154848>.
- (16) Khalil, I. E.; Fonseca, J.; Reithofer, M. R.; Eder, T.; Chin, J. M. Tackling orientation of metal-organic frameworks (MOFs): The quest to enhance MOF performance. *Coord. Chem. Rev.* **2023**, *481*, 215043. DOI: <https://doi.org/10.1016/j.ccr.2023.215043>.
- (17) Mohan, B.; Dhiman, D.; Virender; Mehak; Priyanka; Sun, Q.; Jan, M.; Singh, G.; Raghav, N. Metal-organic frameworks (MOFs) structural properties and electrochemical detection capability for cancer biomarkers. *Microchem. J.* **2023**, 108956. DOI: <https://doi.org/10.1016/j.microc.2023.108956>.
- (18) Deng, G.; Sun, M.; Shi, Y.; Feng, Y.; Lv, Y.; Tang, L.; Gao, J.; Song, P. Construction of MXene/MOFs nano-coatings on PU sponge with enhanced interfacial interaction and fire resistance towards efficient removal of liquid hazardous chemicals. *J. Cleaner Prod.* **2023**, *403*, 136887. DOI: <https://doi.org/10.1016/j.jclepro.2023.136887>.
- (19) Pan, Y.-T.; Zhang, Z.; Yang, R. The rise of MOFs and their derivatives for flame retardant polymeric materials: A critical review. *Compos. Part B-Eng.* **2020**, *199*, 108265. DOI: <https://doi.org/10.1016/j.compositesb.2020.108265>.
- (20) Wang, R.; Chen, Y.; Liu, Y.; Ma, M.; Hou, Y.; Chen, X.; Ma, Y.; Huang, W. Synthesis of sugar gourd-like metal organic framework-derived hollow nanocages nickel molybdate@cobalt-nickel layered double hydroxide for flame retardant polyurea. *J. Colloid Interface Sci.* **2022**, *616*, 234-245. DOI: <https://doi.org/10.1016/j.jcis.2022.01.101>.
- (21) Zhou, X.; Mu, X.; Cai, W.; Wang, J.; Chu, F.; Xu, Z.; Song, L.; Xing, W.; Hu, Y. Design of Hierarchical NiCo-LDH@PZS Hollow Dodecahedron Architecture and Application in High-Performance Epoxy Resin with Excellent Fire Safety. *ACS Appl. Mater. Inter.* **2019**, *11* (44), 41736-41749. DOI: 10.1021/acsami.9b16482.
- (22) Zhang, Z.; Li, X.; Yuan, Y.; Pan, Y.-T.; Wang, D.-Y.; Yang, R. Confined Dispersion of Zinc Hydroxystannate Nanoparticles into Layered Bimetallic Hydroxide Nanocapsules and Its Application in Flame-Retardant Epoxy Nanocomposites. *ACS Appl. Mater. Inter.* **2019**, *11* (43), 40951-40960. DOI: 10.1021/acsami.9b15393.
- (23) Yuan, B.; Zhao, H.; Yang, F.; Zhang, J.; Wu, Y.; Qi, C.; Tan, Z.; Zhang, G.; Ren, B.; Xiao, F. The design of a metal-organic framework with flame-retardant performance and bionic hydrophobic surface inspired by the lotus leaf. *New J. Chem.* **2022**, *46* (37), 17874-17879,

10.1039/D2NJ03190F. DOI: 10.1039/D2NJ03190F.

- (24) Zhao, H.; Yuan, B.; Zhan, Y.; Yang, F.; Zhou, J.; Qi, C.; Lei, C.; Li, Y. Upgrading the pore-size scale of MIL-53 from microporous to macroporous for adsorbing triethyl phosphate and reducing the fire risk of polystyrene. *Part A Appl. Sci. Manuf.* **2022**, *159*, 107003. DOI: <https://doi.org/10.1016/j.compositesa.2022.107003>.
- (25) Wang, X.; Wu, T.; Hong, J.; Dai, J.; Lu, Z.; Yang, C.; Yuan, C.; Dai, L. Organophosphorus modified hollow bimetallic organic frameworks: Effective adsorption and catalytic charring of pyrolytic volatiles. *Chem. Eng. J.* **2021**, *421*, 129697. DOI: <https://doi.org/10.1016/j.cej.2021.129697>.
- (26) Seidi, F.; Jouyandeh, M.; Taghizadeh, M.; Taghizadeh, A.; Vahabi, H.; Habibzadeh, S.; Formela, K.; Saeb, M. R. Metal-Organic Framework (MOF)/Epoxy Coatings: A Review. *Materials* **2020**, *13* (12), 2881.
- (27) Hou, C.-C.; Wang, Y.; Zou, L.; Wang, M.; Liu, H.; Liu, Z.; Wang, H.-F.; Li, C.; Xu, Q. A Gas-Steamed MOF Route to P-Doped Open Carbon Cages with Enhanced Zn-Ion Energy Storage Capability and Ultrastability. *Adv. Mater.* **2021**, *33* (31), 2101698. DOI: <https://doi.org/10.1002/adma.202101698>.
- (28) Wei, Y.-S.; Zhang, M.; Kitta, M.; Liu, Z.; Horike, S.; Xu, Q. A Single-Crystal Open-Capsule Metal–Organic Framework. *J. Am. Chem. Soc.* **2019**, *141* (19), 7906-7916. DOI: 10.1021/jacs.9b02417.
- (29) Song, K.; Li, X.; Pan, Y.-T.; Hou, B.; Rehman, Z. U.; He, J.; Yang, R. The influence on flame retardant epoxy composites by a bird's nest-like structure of Co-based isomers evolved from zeolitic imidazolate framework-67. *Polym. Degrad. Stab.* **2023**, *211*, 110318. DOI: <https://doi.org/10.1016/j.polymdegradstab.2023.110318>.
- (30) Song, K.; Pan, Y.-T.; He, J.; Yang, R. Coordination bond cleavage of metal–organic frameworks and application to flame-retardant polymeric materials. *Ind. Chem. Mater.* **2024**, 10.1039/D3IM00110E. DOI: 10.1039/D3IM00110E.
- (31) Song, K.; Wang, Y.; Ruan, F.; Liu, J.; Li, N.; Li, X. Effects of a Macromolecule Spirocyclic Inflatable Flame Retardant on the Thermal and Flame Retardant Properties of Epoxy Resin. *Polymers* **2020**, *12* (1), 132. DOI: 10.3390/polym12010132.
- (32) Kim, S.-K.; Wie, J. J.; Mahmood, Q.; Park, H. S. Anomalous nanoinclusion effects of 2D MoS₂ and WS₂ nanosheets on the mechanical stiffness of polymer nanocomposites. *Nanoscale* **2014**, *6* (13), 7430-7435, 10.1039/C4NR01208A. DOI: <https://doi.org/10.1039/C4NR01208A>.
- (33) Lin, R.; Ge, L.; Hou, L.; Strounina, E.; Rudolph, V.; Zhu, Z. Mixed Matrix Membranes with Strengthened MOFs/Polymer Interfacial Interaction and Improved Membrane Performance. *ACS Appl. Mater. Inter.* **2014**, *6* (8), 5609-5618. DOI: 10.1021/am500081e.
- (34) Li, Y.; Yang, B.; Yu, Z.; Wang, S.; Wang, Q. A study on effects of stone–thrower–wales defective carbon nanotubes on glass transition temperature of polymer composites using molecular dynamics simulations. *Comput. Mater. Sci* **2021**, *186*, 110005. DOI: <https://doi.org/10.1016/j.commatsci.2020.110005>.
- (35) Rao, W.; Zhao, P.; Yu, C.; Zhao, H.-B.; Wang, Y.-Z. High strength, low flammability, and smoke suppression for epoxy thermoset enabled by a low-loading phosphorus-nitrogen-silicon compound. *Compos. Part B-Eng.* **2021**, *211*, 108640. DOI:

<https://doi.org/10.1016/j.compositesb.2021.108640>.

- (36) Vahabi, H.; Kandola, B. K.; Saeb, M. R. Flame Retardancy Index for Thermoplastic Composites. *Polymers* **2019**, *11* (3), 407.
- (37) Wei, Z.; Chen, X.; Jiao, C.; Ma, M. Research on the fire safety effect of thermoplastic polyurethane elastomer based on sodium fumarate. *Polym. Adv. Technol.* **2021**, *32* (9), 3795-3803. DOI: <https://doi.org/10.1002/pat.5401>.
- (38) Hou, Y.; Qiu, S.; Xu, Z.; Chu, F.; Liao, C.; Gui, Z.; Song, L.; Hu, Y.; Hu, W. Which part of metal-organic frameworks affects polymers' heat release, smoke emission and CO production behaviors more significantly, metallic component or organic ligand? *Compos. Part B-Eng.* **2021**, *223*, 109131. DOI: <https://doi.org/10.1016/j.compositesb.2021.109131>.
- (39) Zhang, F.; Li, X.; Yang, L.; Zhang, Y.; Zhang, M. A Mo-based metal-organic framework toward improving flame retardancy and smoke suppression of epoxy resin. *Polym. Adv. Technol.* **2021**, *32* (8), 3266-3277. DOI: <https://doi.org/10.1002/pat.5338>.
- (40) Zhang, S.; Liu, X.; Jin, X.; Li, H.; Sun, J.; Gu, X. The novel application of chitosan: Effects of cross-linked chitosan on the fire performance of thermoplastic polyurethane. *Carbohydr. Polym.* **2018**, *189*, 313-321. DOI: <https://doi.org/10.1016/j.carbpol.2018.02.034>.
- (41) Xie, M.; He, J.; Li, X.; Yang, R. Ammonium polyphosphate/montmorillonite nanocomposite with a completely exfoliated structure and charring-foaming agent flame retardant thermoplastic polyurethane. *Materials Science and Engineering: B* **2022**, *283*, 115825. DOI: <https://doi.org/10.1016/j.mseb.2022.115825>.
- (42) Wang, R.; Chen, Y.; Liu, Y.; Ma, M.; Tong, Z.; Chen, X.; Bi, Y.; Huang, W.; Liao, Z.; Chen, S.; et al. Metal-organic frameworks derived ZnO@MOF@PZS flame retardant for reducing fire hazards of polyurea nanocomposites. *Polym. Adv. Technol.* **2021**, *32* (12), 4700-4709. DOI: <https://doi.org/10.1002/pat.5462>.
- (43) Cai, W.; Wang, B.; Liu, L.; Zhou, X.; Chu, F.; Zhan, J.; Hu, Y.; Kan, Y.; Wang, X. An operable platform towards functionalization of chemically inert boron nitride nanosheets for flame retardancy and toxic gas suppression of thermoplastic polyurethane. *Compos. Part B-Eng.* **2019**, *178*, 107462. DOI: <https://doi.org/10.1016/j.compositesb.2019.107462>.
- (44) Unnikrishnan, V.; Zabihi, O.; Li, Q.; Ahmadi, M.; Yadav, R.; Kalali, E. N.; Tanwar, K.; Kiziltas, A.; Blanchard, P.; Wang, D.-Y.; et al. Organophosphorus-Functionalized Zirconium-Based Metal-Organic Framework Nanostructures for Improved Mechanical and Flame Retardant Polymer Nanocomposites. *ACS Appl. Nano Mater.* **2021**, *4* (12), 13027-13040. DOI: 10.1021/acsanm.1c02503.
- (45) Sun, Y.; Yu, B.; Liu, Y.; Bai, F.; Yan, J.; Wang, J.; Huang, F.; Gao, S. Design of 2d charring-foaming agent for highly efficient intumescent flame retardant polylactic acid composites. *Compos. Commun.* **2023**, *43*, 101720. DOI: <https://doi.org/10.1016/j.coco.2023.101720>.
- (46) Bi, X.; Di, H.; Liu, J.; Meng, Y.; Song, Y.; Meng, W.; Qu, H.; Fang, L.; Song, P.; Xu, J. A core-shell-structured APP@COFs hybrid for enhanced flame retardancy and mechanical property of epoxy resin (EP). *Adv. Compos. Hybrid Mater.* **2022**, *5* (3), 1743-1755. DOI: 10.1007/s42114-021-00411-0.
- (47) Qi, L.; Cai, W.; Zhang, W.; Wang, B.; Li, W.; Jin, X.; Chen, L.; Yu, B.; Hu, Y.; Xing, W. Application of Silver-Loaded Halloysite Nanotubes in Flame Retardant and Smoke-

- Suppressive Coating for Polyester-Cotton Fabric. *ACS Appl. Mater. Inter.* **2023**, *15* (19), 23725-23735. DOI: 10.1021/acsami.3c02139.
- (48) Sun, Y.; Yu, B.; Liu, Y.; Yan, J.; Xu, Z.; Cheng, B.; Huang, F.; Wang, J. Bio-inspired surface manipulation of halloysite nanotubes for high-performance flame retardant polylactic acid nanocomposites. *Nano Res.* **2023**. DOI: 10.1007/s12274-023-6050-y.
- (49) Yu, S.; Cheng, C.; Li, K.; Wang, J.; Wang, Z.; Zhou, H.; Wang, W.; Zhang, Y.; Quan, Y. Fire-safe epoxy composite realized by MXenes based nanostructure with vertically arrayed MOFs derived from interfacial assembly strategy. *Chem. Eng. J.* **2023**, *465*, 143039. DOI: <https://doi.org/10.1016/j.cej.2023.143039>.
- (50) Zhang, M.; Ding, X.; Zhan, Y.; Wang, Y.; Wang, X. Improving the flame retardancy of poly(lactic acid) using an efficient ternary hybrid flame retardant by dual modification of graphene oxide with phenylphosphinic acid and nano MOFs. *J. Hazard. Mater.* **2020**, *384*, 121260. DOI: <https://doi.org/10.1016/j.jhazmat.2019.121260>.
- (51) Zhang, J.; Li, Z.; Qi, X.; Zhang, W.; Wang, D.-Y. Size tailored bimetallic metal-organic framework (MOF) on graphene oxide with sandwich-like structure as functional nano-hybrids for improving fire safety of epoxy. *Compos. Part B-Eng.* **2020**, *188*, 107881. DOI: <https://doi.org/10.1016/j.compositesb.2020.107881>.
- (52) Zhang, G.; Wu, W.; Yao, M.; Wu, Z.; Jiao, Y.; Qu, H. Novel triazine-based metal-organic frameworks: Synthesis and multifunctional application of flame retardant, smoke suppression and toxic attenuation on EP. *Mater. Des.* **2023**, *226*, 111664. DOI: <https://doi.org/10.1016/j.matdes.2023.111664>.
- (53) Huang, J.; Guo, W.; Wang, X.; Niu, H.; Song, L.; Hu, Y. Combination of cardanol-derived flame retardant with SiO₂@MOF particles for simultaneously enhancing the toughness, anti-flammability and smoke suppression of epoxy thermosets. *Compos. Commun.* **2021**, *27*, 100904. DOI: <https://doi.org/10.1016/j.coco.2021.100904>.
- (54) Song, K.; Wang, Y.; Ruan, F.; Yang, W.; Fang, Z.; Zheng, D.; Li, X.; Li, N.; Qiao, M.; Liu, J. Synthesis of a Reactive Template-Induced Core-Shell PZS@ZIF-67 Composite Microspheres and Its Application in Epoxy Composites. *Polymers* **2021**, *13* (16), 2646. DOI: 10.3390/polym13162646.
- (55) Song, K.; Li, Q.; Yuan, Y.; Hu, S.; Liu, J.; Zhang, Y.; Pan, Y.-T.; Zhao, W.; He, J. Hollow Nanospheres of Red Phosphorus for Fireproof Flexible Sensors Fabricated via 3D Printing. *ACS Appl. Nano Mater.* **2022**, *5* (12), 18080-18092. DOI: 10.1021/acsanm.2c04019.
- (56) Gu, H.; Guo, J.; Wei, H.; Guo, S.; Liu, J.; Huang, Y.; Khan, M. A.; Wang, X.; Young, D. P.; Wei, S. Strengthened magnetoresistive epoxy nanocomposite papers derived from synergistic nanomagnetite-carbon nanofiber nanohybrids. *Adv. Mater.* **2015**, *27* (40), 6277-6282.

Table of Contents (TOC)

